Journal of Materials Research and Technology 36 (2025) 5598–5610

Contents lists available at ScienceDirect

Journal of Materials Research and Technology

journal homepage: www.elsevier.com/locate/jmrt

Refinement of ultrahigh aspect ratio pure aluminum through novel hydrostatic twist extrusion: microstructural and mechanical insights

E. Taherkhani [a,b], M.R. Sabour [a], A. Esmaeilnia [c], A. Jalali Aghchai [b], B. Straumal [d], G. Faraji [a,*]

[a] School of Mechanical Engineering, College of Engineering, University of Tehran, Tehran, Iran
[b] Department of Mechanical Engineering, K. N. Toosi University of Technology, Tehran, Iran
[c] Mechanical Engineering Department, Amirkabir University of Technology, Hafez Av., Tehran, 15875-4413, Iran
[d] Institute of Nanotechnology, Karlsruhe Institute of Technology, Hermann-von-Helmholtz-Platz 1, Eggenstein-Leopoldshafen, 76344, Germany

ARTICLE INFO

Handling editor: M Meyers

Keywords:
Hydrostatic twist extrusion (HTE)
High angle grain boundary (HAGB)
Electron backscatter diffraction (EBSD)
Grain refinement
Mechanical properties
Aluminum

ABSTRACT

Hydrostatic Twist Extrusion (HTE), a recently introduced Severe Plastic Deformation (SPD) technique, enables the refinement of pure aluminum billets with an ultrahigh aspect ratio, exceeding the limitations of conventional SPD methods. In this study, the microstructural and mechanical properties of HTE-processed aluminum were examined through Electron Backscatter Diffraction (EBSD), tensile testing, and hardness measurements. EBSD analysis revealed that HTE effectively reduced the grain size from approximately 99 μm–4.9 μm after two passes, with the formation of a lamellar structure. Additionally, the HTE process led to a considerable increase in the fraction of high-angle grain boundaries (HAGBs), with the HAGB fraction increasing from 33.4 % after the first pass to 56.7 % after the second pass. The application of high hydrostatic pressure during processing was key in accelerating the formation of HAGBs, contributing to enhanced microstructural properties. Following one pass, microhardness rose to around 43.7 HV, and further increased to 52.4 HV after two passes, from an initial 25.6 HV. Meanwhile, the total ductility loss was 14 % after the first pass and 10 % after the second. The results suggest that the strengthening mechanism in HTE-processed aluminum is primarily driven by grain boundary strengthening, dislocation interactions, and the beneficial effects of high hydrostatic pressure, which together enhance both strength and ductility. The study highlights the effectiveness of HTE in achieving a balanced combination of strength and ductility, making it a promising technique for the processing of ultrahigh aspect ratio pure aluminum.

1. Introduction

Grain size is a crucial microstructural attribute influencing nearly every aspect of the physical and mechanical behavior of polycrystalline metals, as well as their chemical and biochemical interactions with the environment [1]. As a result, controlling grain size has long been recognized as an effective method for engineering materials with targeted attributes. As the demand for superior material performance continues, efforts to refine microstructures through new forming techniques continue to evolve. Conventional metal forming techniques, including rolling, forging, and extrusion, generally result in plastic strains below 2.0 [2]. When techniques such as multi-pass rolling, drawing, or extrusion exceed a strain of 2.0, the material's thickness or diameter becomes excessively thin, making it unsuitable for structural applications. To overcome this limitation, severe plastic deformation (SPD) methods have been developed to induce very high strains in bulk metals without changing their geometry [3,4]. In other words, the objective of SPD is to maintain the sample's shape while altering its internal microstructure.

An SPD process is defined as a metal forming method performed under extensive hydrostatic pressure, capable of applying very high strain to a bulk sample while preserving its overall dimensions and facilitating exceptional grain refinement [5]. The purpose of applying high hydrostatic pressure is to inhibit crack propagation and postpone failure. Techniques such as Equal Channel Angular Pressing (ECAP) [6–10], High-Pressure Torsion (HPT) [11–15], Accumulative Roll-Bonding (ARB) [16–18], Cyclic Extrusion Compression (CEC) [19–21], Twist Extrusion (TE) [22,23], Cyclic Extrusion Expansion

* Corresponding author.
E-mail address: ghfaraji@ut.ac.ir (G. Faraji).

https://doi.org/10.1016/j.jmrt.2025.04.179
Received 8 March 2025; Received in revised form 12 April 2025; Accepted 16 April 2025
Available online 16 April 2025

(CEE) [24], Hydrostatic tube cyclic expansion extrusion (HTCEE) [25], Tubular Channel Angular Pressing (TCAP) [26], Parallel Tubular Channel Angular Pressing (PTCAP) [27], and Friction-Stir Processing (FSP) [28–30] are considered some of the most significant and thoroughly researched severe plastic deformation (SPD) methods. Additionally, SPD-derived metal forming techniques like Hydrostatic Extrusion (HE) and the KoBo method have demonstrated the capability to produce ultrafine-grained (UFG) or nanocrystalline (NC) microstructures in metallic materials [31–34]. SPD technologies are becoming more widely adopted for their unique ability to achieve grain size refinement down to the sub-micrometer and nanometer scales. One key benefit of grain size refinement is the increased yield strength, which enhances the elastic behavior of the metal according to the Hall–Petch principle [35,36]. Enhanced fatigue properties are another advantage of UFG materials, resulting from the high density of grain boundaries that obstruct the advancement of cracks [37]. Since Segal introduced the ECAP process in 1974 [38], SPD has garnered renewed interest in metallurgy as it enables the application of nearly infinite shear strain to a metal in a repetitive manner. The observation of UFG microstructure development through SPD was another significant breakthrough, initially identified by Bridgman using X-ray diffraction (XRD) [39,40]. The contributions of Valiev's group brought significant attention to the potential of SPD methods in enhancing metallic materials, demonstrating how the extreme grain refinement from SPD processing leads to improved strength across different metals and alloys [41,42]. Well-explored methods like ECAP, ARB, and HPT are commonly used to produce ultrafine-grained metals. These processes result in metals with average grain sizes less than 1 μm and primarily high-angle misorientation at the grain boundaries. These microstructural modifications achieved through SPD processing enhance the properties of materials, broadening their applicability in diverse fields including biomedical implants, automotive manufacturing, electronics, energy production, and sports equipment [43–46]. For example, Titanium alloys with ultrafine grains created through SPD techniques exhibit enhanced biocompatibility and mechanical performance compared to traditional titanium alloys [1].

Despite their notable mechanical properties, a significant limitation of SPD pressing techniques lies in the high processing forces, which cause punch buckling or yielding, thereby restricting the sample's length-to-diameter ratio and limiting their utility in industrial applications [43,47]. In this regard, reducing the friction in SPD methods allows the processing of samples with long lengths. One of the outstanding solutions is the implementation of hydrostatic SPD methods. Hydrostatic SPD methods refer to those methods in which fluid is used to reduce the friction between the die and the sample and allow the production of long samples [48]. Moreover, metals with nanocrystalline or UFG structures often show limited tensile ductility at room temperature, even when the same metals are highly ductile at traditional grain sizes [49,50]. Thus, another significant disadvantage of SPD-processed materials is their pronounced reduction in ductility, which is essential for engineering applications due to its impact on manufacturability and functional performance. As a case in point, Siahsarani and Faraji developed hydrostatic cyclic extrusion–compression as a new severe plastic deformation technique for refining ultrafine-grained commercial pure aluminum rods [51]. Their findings revealed a marked decrease in total elongation, dropping from the initial 26 %–14 % after the first pass and further to 13 % after the second pass. Another study applied accumulative back extrusion (ABE) to commercially pure aluminum, producing an ultrafine microstructure [52]. The results indicated a substantial reduction in uniform elongation, which decreased from 19 % in the annealed material to 3 %, 5 %, and 4 % after one, two, and three passes of ABE, respectively. Multi-pass PTCAP was applied to commercial Al-6061 alloy tubes to evaluate the effects of processing passes on grain refinement and mechanical characteristics [53]. The annealed material had a UTS of ~116 MPa and an elongation of 43 %, attributed to the heat treatment before PTCAP. Grain refinement increased the UTS to 179 MPa after one pass, while elongation declined drastically to 16.3 % (a reduction of 62 %). After two PTCAP passes, the UTS reached around 180 MPa with elongation reducing slightly further to 16 %.

It is apparent that while microstructure refinement enhances certain properties, it significantly diminishes ductility, limiting the practical applications of the processed sample. According to several studies, a potential solution to this issue involves utilizing fluid as an intermediary medium between the die and the sample, a technique referred to as hydrostatic SPD methods. Using fluid not only enhances the aspect ratio (length/diameter) of the samples [54,55] but also minimizes ductility loss [48]. Recently, hydrostatic twist extrusion (HTE) has been presented by Haghpanah et al. [55] to produce a long square cross-section sample. The HTE method was developed based on a well-known SPD method called twist extrusion invented by Beygelzimer et al. [22], to solve the length limitation by conducting fluid, which limits the metal-to-metal contact only to the deformation zone. However, the novel HTE process has not been extensively studied to evaluate its influence on microstructure and mechanical properties over multiple passes. This research explores the changes in mechanical properties through tensile and microhardness testing, along with microstructural analysis via Electron Backscatter Diffraction (EBSD), in samples processed through different passes of hydrostatic twist extrusion (HTE) as a novel SPD method.

2. Experimental procedure

This study involved conducting the HTE process in three passes to assess its potential as a novel SPD method for producing long ultrafine-grained billets at room temperature. The samples were made from commercially pure aluminum (composition detailed in Table 1), machined to dimensions of 15 mm × 15 mm in cross-section and 100 mm in length. They were then annealed at 300 °C for 1 h to produce a homogeneous and recrystallized microstructure.

Fig. 1 highlights the equipment, the fabricated die, and the sequential steps of the HTE method, with the dies being machined from tool steel and having a hardness of 58 HRC. The process begins with placing the sample in the inlet channel, where the fluid fills the space around it, followed by positioning the backward punch in the outlet channel, see Fig. 1a. To prevent fluid leakage during the second step, a polytetrafluoroethylene (PTFE) seal with a larger diameter than the initial channel was designed and incorporated into the process. In the second step, the punch moves downward, causing the fluid to become pressurized (Fig. 1b). Further descent of the punch then pushes the sample into the deformation zone. This process continues until the bottom of the sample makes contact with the backward punch, ensuring the deformation zone is fully occupied by the sample. In the final stage, the backward punch is taken out, allowing the punch to press the sample down until it entirely moves through the deformation zone (Fig. 1c). Applying higher strain through more HTE passes requires removing the samples from the die and placing them back into the inlet channel to repeat the procedure from the first step.

After completing the HTE process, the aluminum billets were sectioned perpendicular to their longitudinal axis. The resulting sections were then prepared using standard metallographic techniques. Optical microscopy (OM) was used to characterize the microstructure of the original sample. To observe it, the specimens were polished to a mirror-like surface with silica and alumina powder. The specimens were then electrochemically etched at room temperature and $V = 20$ V for 40 min

Table 1
Composition of commercially pure aluminum measured in wt.%.

Al	Si	Fe	Cu	Mn	Cr	Zn
99.4	0.198	0.307	0.0049	0.0098	0.0035	0.0113
Ti	Be	Pb	Sb	V	Zr	Mg
0.0154	0.00003	0.00005	0.0006	0.02	0.0008	0.0048

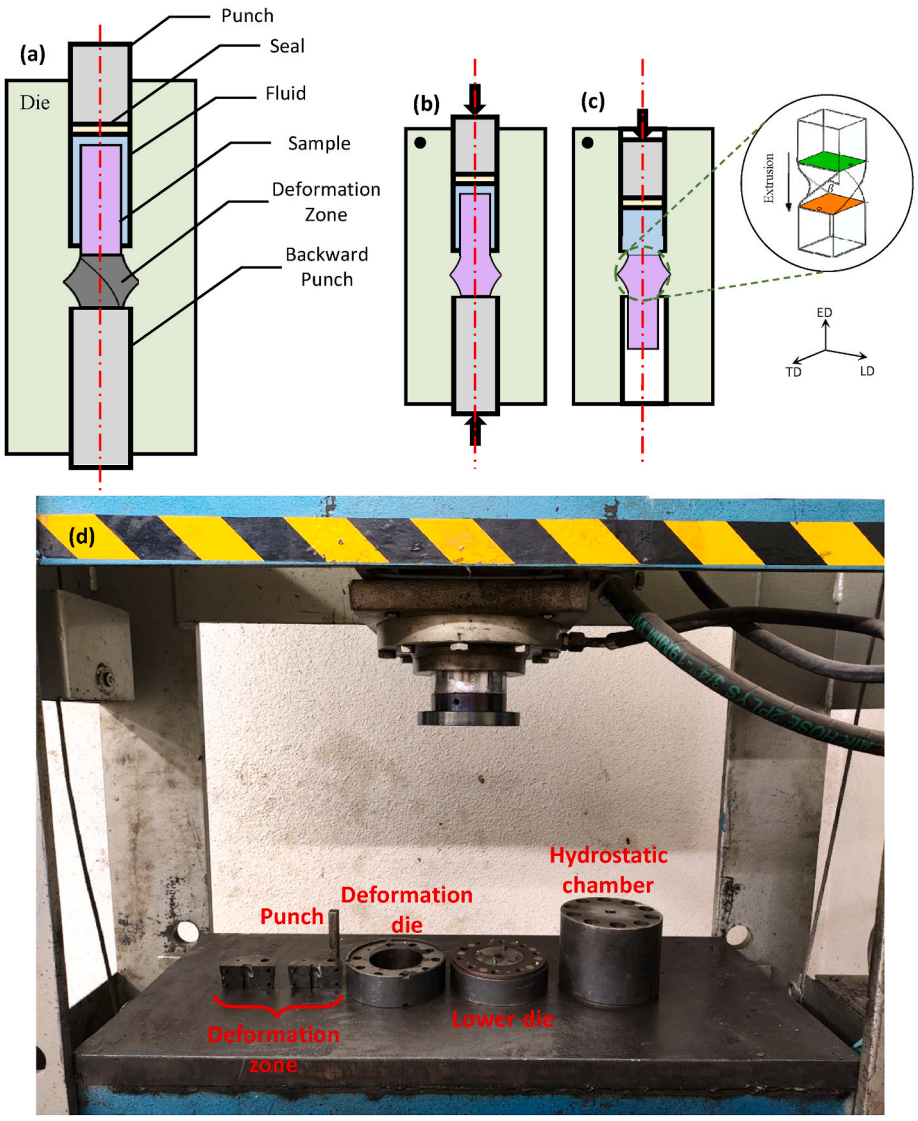

Fig. 1. Die component of the HTE method and different steps of processing a) first step, b) second step, c) third step, and d) experimental set up and die components (ED, TD, and LD refer to the extrusion direction, transverse direction, and longitudinal, respectively).

using a solution composed of 10 ml fluoboric acid (HBF_4) and 200 ml distilled water. The microstructural changes following the HTE process were examined using electron backscatter diffraction (EBSD) analysis at 1.5 mm away from the surface. Samples for EBSD were prepared by polishing the surface down to 0.25 μm diamond paste followed by electro-polished with a 30 % HNO_3 solution in methanol, working at $V =$ 15 V and a temperature of −20 °C. A FEG-SEM operated at 20 kV and equipped with an EBSD detector was utilized for microstructure evolution after the HTE process. The step size for scanning was 0.3 μm. The recorded data sets were indexed using the EDAX orientation imaging microscopy (OIM 8.0) software. To evaluate the mechanical properties, tensile testing was carried out on the samples at room temperature, both before and following the process. In this regard, tensile test samples were machined 1.5 mm away from the surface of the HTE-processed billets along the ED. Also, X-ray diffraction (XRD) analysis was performed using a Cu-Kα radiation source to evaluate the dislocation density of the HTE-processed pure aluminum samples. The measurements were conducted over a 2θ range of 5°–100° with a step size of 0.04°. Dislocation density was estimated based on peak broadening using the Williamson–Hall method. A Santam tensile machine was utilized to conduct the test, operating at a strain rate of 0.5 mm/min. Microhardness was measured on the specimens with a Vickers hardness tester under a 100 g load for 10 s. The hardness was evaluated from the surface to the center to determine the homogeneity across the cross-section of the processed samples. To better visualize the microhardness distribution, measurements were taken across the entire cross-section, and color maps were generated for both the unprocessed and processed billets. Field emission scanning electron microscopy (FE-SEM) was used to examine the mechanism of sample failure, and subsequently, images of the fracture cross-section were taken using a HITACHI S-4160.

3. Results and discussion

In Fig. 2a, the aluminum sample is illustrated after completing two passes of the HTE process. It can be observed that a 100 mm length sample, with an aspect ratio close to 4.8, was processed. The presence of fluid between the upper channel and the sample leads to a high aspect ratio by substantially reducing the frictional force. Regarding this, the processing load necessary for completing the deformation process consists of three components, as outlined in Eq. (1).

$$F_T = F_D + F_f + F_R \tag{1}$$

F_D, F_f, and F_R represent the loads required for deformation, friction, and redundant work, respectively. In both conventional and hydrostatic

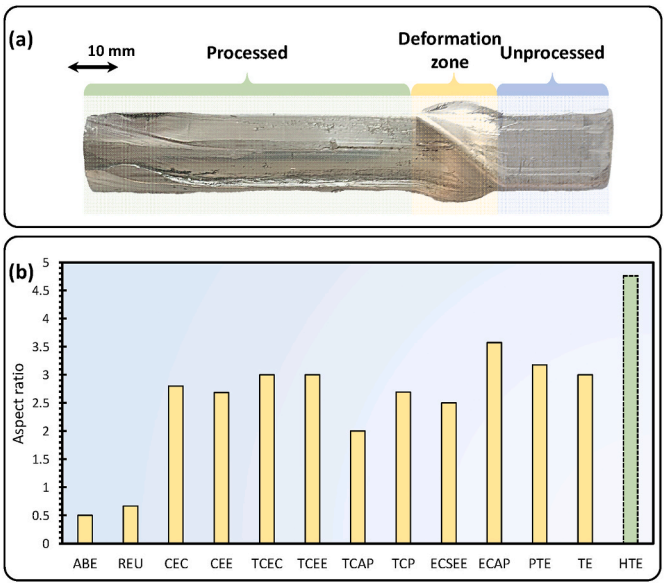

Fig. 2. a) Image of the processed sample via two passes of HTE, and b) compression between aspect ratio (length/diameter) of processed pure Al via various methods (data are gathered from Ref.s [56–66]).

SPD methods, the deformation load (F_D) is nearly the same, while redundant work (F_R) arises from shear stress [48]. However, friction load (F_f) constitutes a large portion of the total load [67], primarily depending on the level of surface contact during the process [48]. The reduction of processing load due to conducting fluid has been widely discussed by researchers through the application of finite element method (FEM) analysis [55,68,69,70]. It should be emphasized that, because of the restricted metal-to-metal contact in hydrostatic SPD methods, the length of the sample does not affect the processing load, meaning that the processing load is independent of the sample length. To better illustrate the role of conducting fluid in HTE processing, Fig. 2b displays the aspect ratios (length/diameter) of samples obtained via multiple methods, including accumulative back extrusion (ABE) [56], repetitive extrusion and upsetting (REU) [57], cyclic extrusion compression (CEC) [58], cyclic expansion extrusion (CEE) [59], tube cyclic extrusion compression (TCEC) [], tube cyclic expansion extrusion (TCEE) [60], tubular channel angular pressing (TCAP) [61], tube channel pressing (TCP) [62], elliptical cross-sectioned spiral equal-channel extrusion (ECSEE) [63], equal channel angular pressing (ECAP) [64], planar twist extrusion (PTE) [65], and twist extrusion (TE) [66]. HTE shows significant potential for processing relatively long samples, making it suitable for industrial applications.

3.1. Microstructure evolution

Fig. 3 displays the OM microstructure of the Al sample before undergoing the HTE process. The annealing treatment led to recrystallization, producing a nearly homogeneous grain distribution with an average size of ~99 μm. To assess the influence of the HTE process on the microstructure of Al samples, EBSD analysis was carried out. Fig. 4 provides a visualization of the microstructural changes following a single pass of the HTE process. The coarse grains of the annealed sample were significantly refined to an average grain size of 6.4 μm due to the severe shear strain induced by the HTE process. Unlike other techniques like ECAP, TE-based methods (i.e., HTE) generate four separate shear planes owing to their uniquely shaped deformation zone, thereby subjecting the sample to intense plastic deformation [71]. The aluminum billet undergoes opposite-direction simple shear at the inlet and outlet of the deformation zone (TD-LD), resembling the shear mechanism in HPT; hence, the macrostructure is anticipated to display elongated structural elements aligned with the vortex direction centered around the extrusion axis [71]. Meanwhile, throughout the deformation zone, it is primarily subjected to simple shear in planes aligned with the extrusion direction (ED-LD and ED-TD). In addition, hydrostatic pressure in HTE plays a crucial role in shaping the deformation zone, facilitating plastic flow uniformity and reducing the likelihood of crack formation [72].

This process also transformed the initial grains of the Al alloy into elongated structures with an average aspect ratio of 0.43 after a single pass. In this context, OM revealed a heavily fibrous structure in the Al–Mg alloy after only one pass of TE processing [72]. It is important to highlight that in cases where grains are either flat or elongated, there is less restriction on strain, enabling slip to occur using fewer than five slip systems [73,74]. Furthermore, Fig. 4a–c illustrate a microstructure characterized by the presence of both high-angle grain boundaries (HAGBs) and low-angle grain boundaries (LAGBs). LAGBs are considered grain boundaries with a misorientation angle between 2° and 15°, while HAGBs are considered grain boundaries with a misorientation angle greater than 15°. It is also worth noting that the elongated grains of the Al alloy sample, after performing four passes of ECAP, were reported through OM analysis [75]. Moreover, the texture resulting from one application of HTE ranged between (1 0 0) and (1 1 1), with larger grains displaying either (1 0 1) or (1 1 1) orientations (Fig. 4d). This variation is depicted as blue and green grains in the inverse pole figure (IPF), see Fig. 4a–c.

In FCC-structured materials, such as aluminum, the stacking fault energy (SFE) is the main factor that defines the primary mechanism for grain refinement. The separation of partial dislocations in materials is governed by their SFE [76,77]. In general, increased SFE leads to a smaller distance between partial dislocations and a thinner stacking fault, thus promoting cross-slip [78,79]. Therefore, in aluminum with a SFE of 135–220 mJ/m^2 [80], grain refinement can be expected to occur primarily through the movement of dislocations. Also, due to

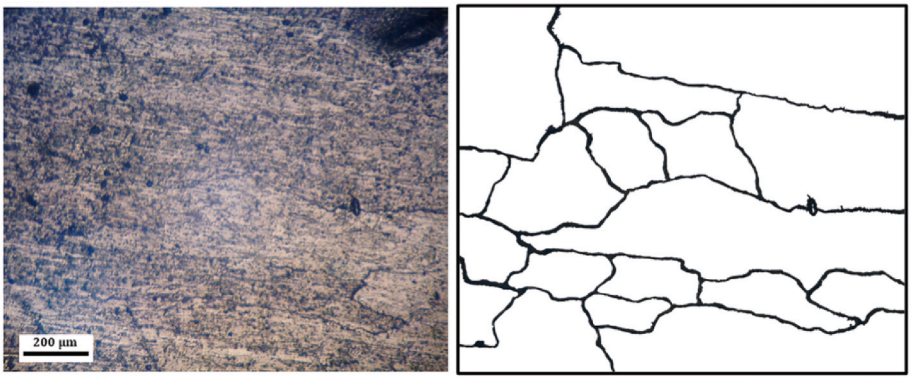

Fig. 3. OM micrograph and grain boundary map of initial Al sample.

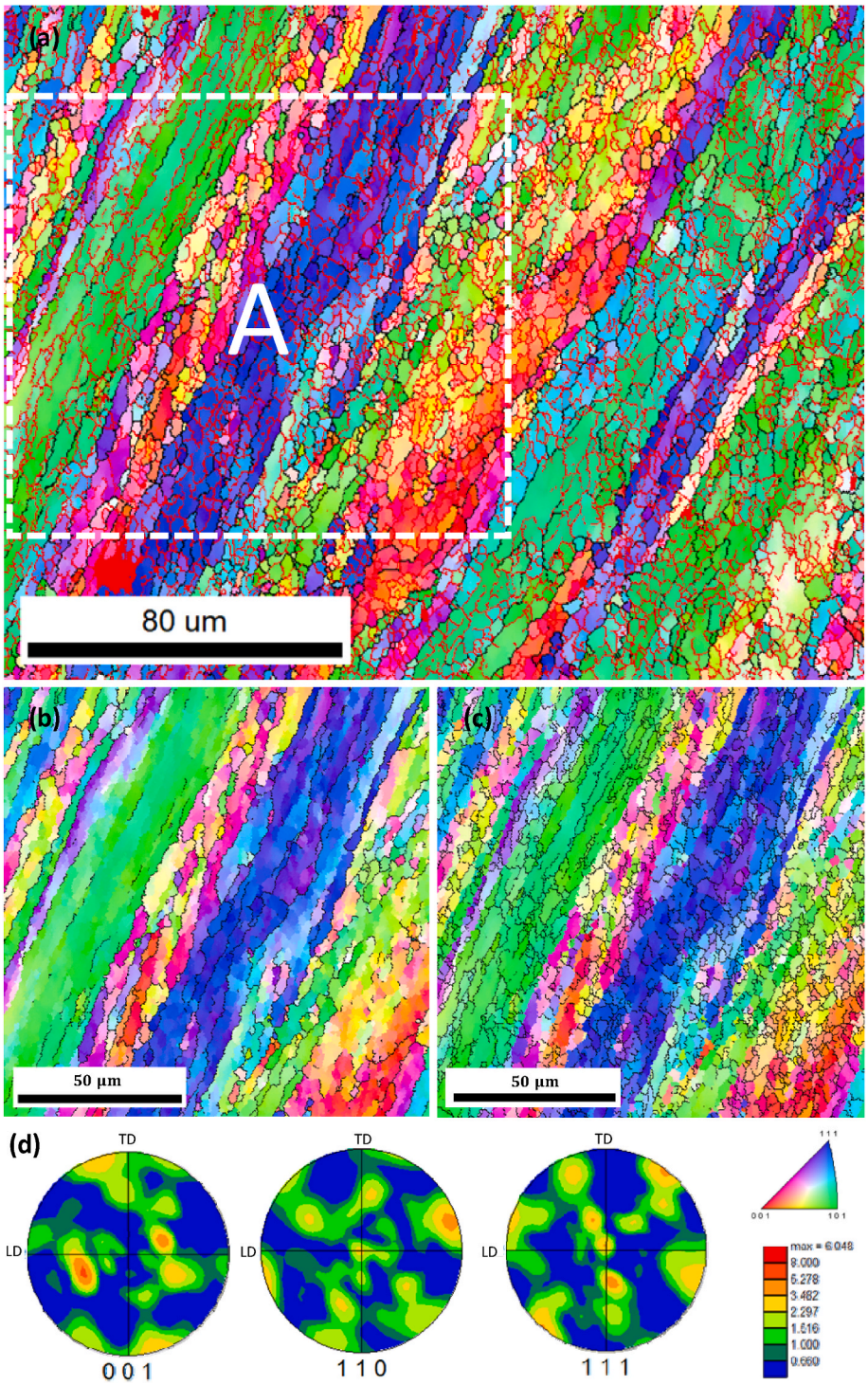

Fig. 4. EBSD microstructure of one pass HTE processed sample showing a) HAGBs and LAGBs, b) HAGBs at area A, c) LAGBs at area A, and d) (0 0 1), (1 1 0), and (1 1 1) corresponding pole figures.

aluminum's high stacking-fault energy, dynamic recovery occurs at a fast rate, diminishing the stored energy required for discontinuous dynamic recrystallization (DDRX), especially in materials where grain boundary mobility is low at room temperature [81]. Extensive studies by various researchers have shown that imposing plastic strain increases dislocation density [25,61,82–84]. It is highlighted that, based on the concept of low-energy dislocation structures (LEDS), the rise in dislocation density during deformation results from the mutual entrapment of dislocations in energetically favorable configurations [73,85,86]. At low levels of strain, geometrically necessary dislocations (GNDs) and statistically stored dislocations (SSD) formed to accommodate plastic deformation [87]. As deformation continued, dislocation walls developed from dislocation networks [88,89], separating the grains into sub-grains (cell blocks) in which fewer slip systems than those outlined by the Taylor criterion are used to accommodate strain [90]. It is worth mentioning that when dislocations are trapped in LEDS, they primarily form into two-dimensional dislocation arrays, i.e. dislocation walls [73]. In terms of sub-grains, it was found that, during the HTCEC processing of

copper tubes, ultrafine cells with an average size of about 993 nm are created, accompanied by a high density of tangled dislocations [82].

As various slip systems in the sub-grains are activated to satisfy the von Mises theory [91,92], the misorientation increases due to the interactions, rearrangements, and entanglements of their dislocations [93]; therefore, as the strain increases, dislocations accumulate significantly at the sub-grain boundaries and dense dislocation walls [94], causing higher misorientation across these areas. In this context, Fig. 5a shows the distribution of misorientation angles throughout the microstructure of the one-pass HTE processed sample. It clearly shows that approximately 72 % of the boundaries are LAGBs and sub-grain boundaries, indicating that the strain is insufficient to convert them into HAGBs. Orlov et al. [95] reported that, after just one pass of conventional TE, approximately 95 % of the boundaries were LAGBs and sub-grain boundaries in regions near the surface, which is 32 % higher than the percentage observed in the HTE process. This is due to the fact that HTE processing applies a greater amount of hydrostatic pressure compared to the TE process. In this regard, McKenzie et al. [96] observed that during ECAP processing, applying a back pressure of 200 MPa increases dislocation density, supporting prior statements.

It should be noted that, Hughes and Hansen have been stated that the development of HAGBs at moderate strain levels (e.g. those seen after the first pass of HTE) is caused by coarse slip occurring as S-bands [97]. They also documented that extended high-angle lamellar boundaries develop at the interfaces between the clustered S-bands and the surrounding matrix, which could be seen in Fig. 4. Another feature revealed through the inverse pole figure of a one-pass HTE processed sample is that the majority of sub-grain boundaries and LAGBs are aligned in a specific direction, see Fig. 4a and b. In this context, Huang and Winther demonstrated that in metals with medium to high SFE, the dislocation structures formed via rolling and tension are predominantly oriented along the shear direction [98,99].

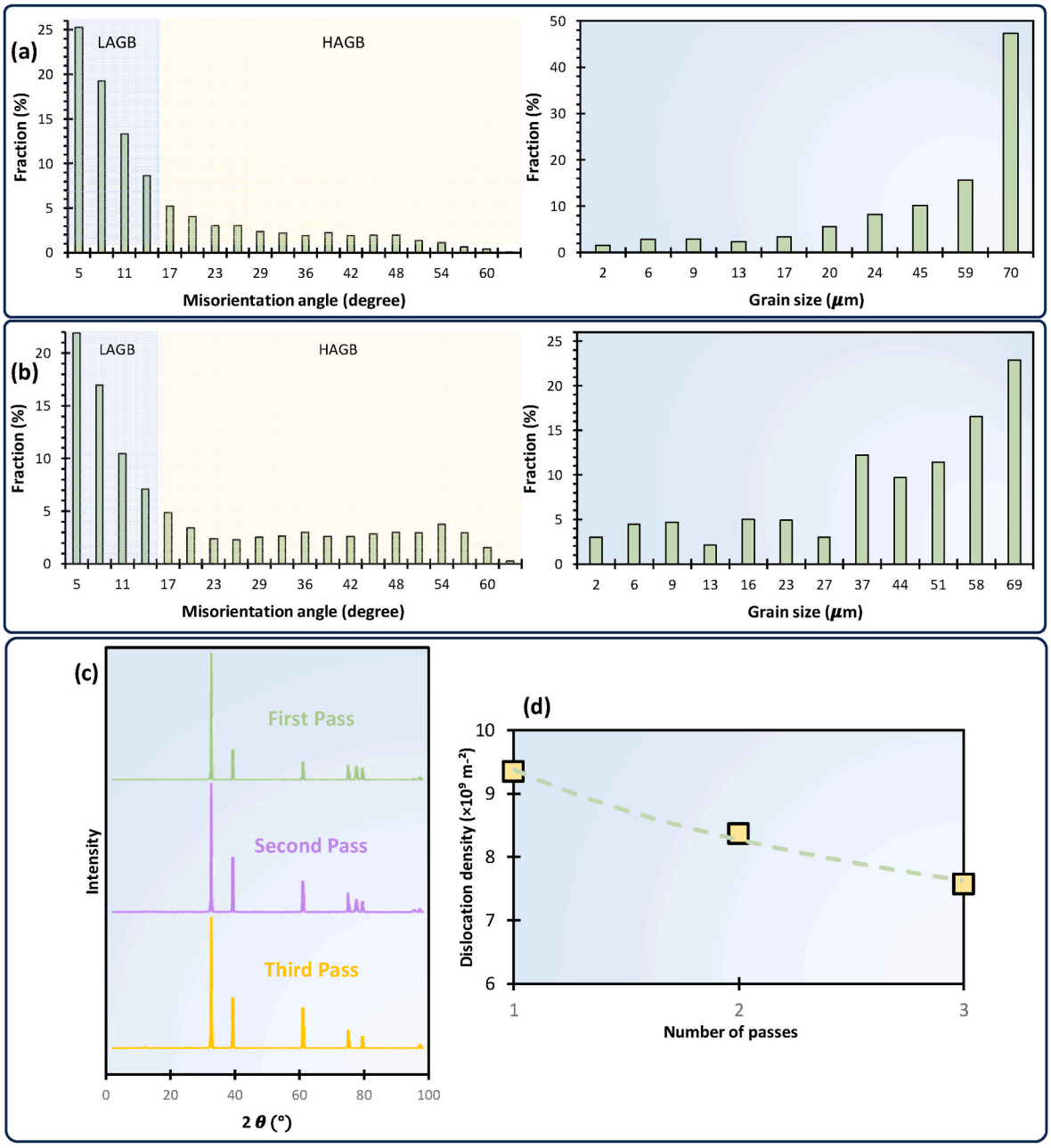

Fig. 5. (a, b) Distribution of misorientation angle and grain size with HAGBs (based on Figs. 4b and 6a) after a) one pass and b) two passes, c) XRD profiles of HTE-processed Al samples, and d) variation in dislocation density with respect to the number of HTE passes.

The microstructure of an Al sample after two passes of the HTE process is shown in Fig. 6. Following Fig. 6a, it is evident that, although most of the grains are elongated with an average aspect ratio of 0.41, several equiaxed grains are also present, and the microstructure contains both LAGBs and HAGBs. It should be noted that the average grain size decreased to 4.9 μm. This is a typical microstructure of deformed Al [84,100]. Additionally, the size of grain with HAGBs after two passes is clearly finer than that achieved after the first pass (Figs. 6a and 4a), with coarser grains have (0 0 1) orientation. Such a texture strengthening is also seen pole figures given in Figs. 4d and 6c. It is clear that due to the higher induced strain after two HTE passes, sub-grain sizes decrease progressively, while misorientation angles across dense dislocation walls increase significantly.

This results in the formation of numerous lamellar sub-grains with lamellar boundaries. In this context, it was confirmed that these lamellar sub-grains tend to align parallel to the direction of shear strain [78,101,102], as illustrated in Fig. 6b. The findings indicate that at higher strains, cell blocks become very flat and are sandwiched by lamellar dislocation boundaries, which have taken the place of dense dislocation walls and double-walled microbands observed at lower strains [103]. The comparison between Figs. 6a and 4b demonstrates that the fraction of HAGBs significantly increases after two HTE passes. Further explanation based on Fig. 5 shows that the fraction of HAGBs increases from approximately 33.4 % after the first pass to around 56.7 % after the second pass of the HTE process, indicating a rise of about 70 %. In other words, unlike the first pass where LAGBs are predominant, HAGBs become predominant after the second HTE pass. Regarding this, Faraji et al. [53] also found that increasing the number of passes leads to a higher fraction of HAGBs, due to the greater strain introduced. Also, based on the increase in the HAGB fraction after the second pass of HTE (Fig. 5), it can be expected that the interface bonding within the lamellar structure is enhanced by further straining through the HTE process, which aligns with the findings reported by Wang et al. [104].

As indicated in Fig. 5, the second pass of HTE results in a higher fraction of angles between roughly 30 ° and 60 ° compared to the first pass. This matter was shown by other researchers [95]. As noted earlier, sub-grains form at the initial stage of deformation and adopt a favorable orientation. As the grain undergoes large rotations, various sections of a grain may end up with different orientations due to grain subdivision caused by dislocation boundaries that form at the start of deformation. As a result of the interaction between dislocation interaction and texture evolution, very high-angle boundaries (e.g. between 40 ° and 60 °) can develop [103,105]. It is important to note that the application of high plastic strain causes the fraction of lamellar boundaries to increase. In addition, the lamellar boundaries become thinner. This phenomenon, associated with a reduction in dislocation density (see Fig. 5c and) at the boundaries, results in an increased misorientation angle along the boundaries and a higher number of HAGBs [105–107]. To illustrate this

Table 2
Values of dislocation density and lattice parameters as determined from the XRD pattern evaluations.

Number of passes	Dislocation density ($\times 10^{12}\ m^{-2}$)	Lattice parameter (nm)
One	9.34	377.88
Two	8.36	420.3
Three	7.56	399.19

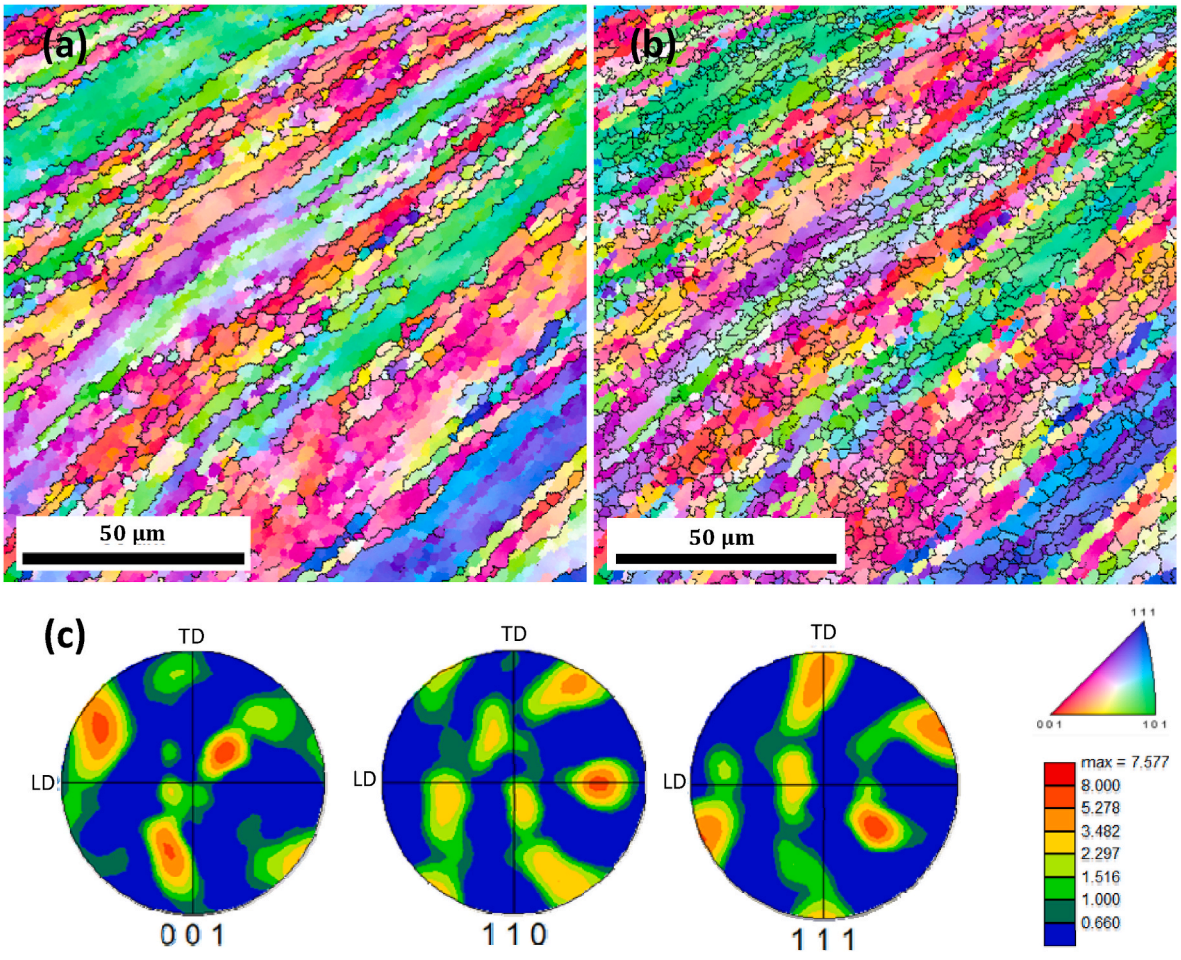

Fig. 6. IPF maps after second pass of HTE showing a) HAGBs, b) LAGBs, and c) (0 0 1), (1 1 0), and (1 1 1) related pole figures.

behavior, Table 2 highlights how dislocation density changes with each additional HTE pass. Mishra et al. [108] observed the thinning of cell boundaries during the ECAP processing of pure Cu as a result of straining, which can be expressed by the equation below.

$$t\,(nm) = 1 + \left(\frac{k}{\gamma}\right)^2 \tag{2}$$

Here, k and γ are constants related to the material and the amount of strain imposed on the sample. As can be seen, applying higher magnitude of strain on sample reduces the thickness of cell boundaries. It should be noted that, while two passes of HTE formed approximately 57 % HAGBs, only 33 % of boundary angles were above 15 ° after four passes of conventional TE (which is almost equivalent to one pass of HTE) [95]. This demonstrates the higher efficiency of the HTE process compared to TE, due to the higher imposed hydrostatic pressure. Regarding this, Meiser et al. [109] through analyzing pure silver, argued that imposing higher hydrostatic pressure increases the Gibbs free energy of boundaries, leading to a greater orientation angle between neighboring grains, which is in good agreement with the achieved results. A similar dependency of misorientation angle on the amount of hydrostatic pressure was also reported by Jahedi et al. [110] during processing pure Cu through high-pressure double torsion.

3.2. Mechanical properties

The engineering stress-strain graphs shown in Fig. 7a, which were conducted at room temperature, depict the behavior of aluminum samples subjected to different HTE passes. Moreover, Fig. 7b clearly illustrates the variations in UTS, YS, and total elongation following different numbers of HTE passes. During the early stages of a tensile test, stress increases sharply as strain is applied to the sample, leading to dislocation generation and accumulation (or formation of sub-grains as

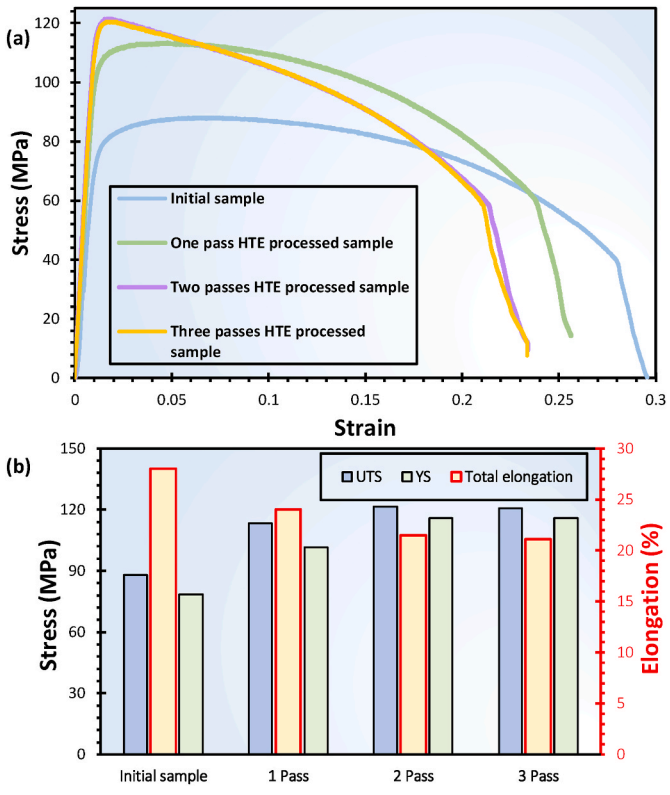

Fig. 7. a) Stress-strain curve related to the samples after performing various pass of HTE process and b) UTS, YS, and elongation of samples processed via various pass of HTE.

observed via IPF images). This, in turn, hinders dislocation movement and increases the likelihood of dislocation interaction. After this initial rise, the rate of strain hardening begins to decrease until it balances with the recovery rate, at which point the stress reaches its maximum value. Beyond this point, the stress decreases because the recovery rate surpasses the strain hardening rate. As can be seen, the occurrence of flow softening is evident after the peak point of stress, regardless of the number of HTE passes. This matter has also been observed by other researchers [52,57]. It was discovered that dynamic recrystallization (DRX) and dynamic recovery (DRV) are the two potential mechanisms responsible for this [111,112]. The term DRX refers to the formation and migration of high-angle grain boundaries, which are driven by the energy accumulated during deformation. However, since the activation energies for the migration of LAGBs are generally about twice those for HAGBs, LAGBs are not expected to migrate at low temperatures but can do so at higher temperatures [113]. Considering the limited possibility of grain boundary migration at room temperature, it is likely that DRV is the dominant mechanism leading to the observed flow softening.

As observed, the aluminum sample subjected to the HTE process shows a significant increase in strength, which further increases with each additional pass. According to the plots, following one pass, the UTS increased from 88 MPa to roughly 113 MPa, while the YS rose from 79 MPa to 102 MPa. Performing a second pass enhances strength, resulting in ultimate tensile strength (UTS) and yield strength (YS) values of 121 MPa and 116 MPa, respectively. Since the average grain size did not undergo a significant reduction after the second pass, the increased strength may be attributed to the higher number of HAGBs formed through further straining [114], as confirmed by Fig. 5. Numerous researchers have highlighted the significant impact of the misorientation angle on the strength of materials [70,115,116]. HAGBs strengthen grain boundaries by increasing the energy required for slip between grains, whereas LAGBs provide minimal resistance to the movement of mobile dislocations. Canadinc et al. [70] outlined the role of dislocation motion in contributing to hardening within the inner areas of grains as well as along the grain boundaries. They discovered that the grain boundary misorientation effect has minimal influence on the hardening rate in CG materials. However, in the UFG and NG range, the hardening rate is significantly higher for larger grain boundary misorientation. The effect of grain boundary misorientation on the hardening rate ($\dot{\rho}$) is illustrated in Eq. (3).

$$\dot{\rho} = \sum_n \sum_q \frac{K}{db}\,(1+\sin\theta)|\dot{\gamma}| \tag{3}$$

In this equation, K, d, and b refer to the geometric constant, the average grain size, and the Burgers vector, respectively. Additionally, θ represents the grain boundary misorientation, and $\dot{\gamma}$ indicates the shear strain rate. The positive impact of HAGB fractions on strength was demonstrated by Canadinc et al. [70] through a comparison of the 4C and 8E ECAP processing methods applied to IF steel. As previously mentioned, increasing strain leads to a reduction in the thickness of cell walls, which could contribute to strengthening. The contribution of cell boundaries involves more than just their impact on dislocation density; as they become thinner, they inhibit dislocation motion and acquire a grain-boundary character, i.e. they can be considered progressively more resistant to dislocation penetration [108]. The strength of a metal is influenced by various factors, which can be quantified using the Hall-Petch equation.

$$\sigma = \sigma_{f\,Al} + \sigma_{dis} + \sigma_{GB} + \sigma_{SS} + \sigma_{Pre} \tag{4}$$

Where, $\sigma_{f\,Al}$, σ_{SS}, and σ_{Pre} stand for friction strength of pure Al, solid solution strengthening, and precipitation strengthening, respectively. Given that this study focuses on pure aluminum, the two latter terms do not influence strengthening in the HTE processing. Work hardening (σ_{dis}) and grain refinement (σ_{GB}) are recognized as the primary contributors to the improvement of mechanical properties [117]. Strength is

enhanced by the work hardening mechanism, which operates through the multiplication (i.e. GND), movement, and interaction of dislocations, which is considered the key strengthening mechanism for metals that experience plastic deformation. When the grain size is reduced to the ultrafine-grained (UFG) regime, it is important to consider that a hardening mechanism constrained by dislocation sources may be at work, demanding higher stress to initiate other dislocation sources [108,118,119]. This is in good agreement with the IPF maps. Along with strengthening from GND-induced work hardening, back-stress effects may also play a role in enhancing the overall strength of the material. Although back-stress is not a commonly observed strengthening mechanism in homogeneous materials [120], in the case of lamellar microstructures, which exhibit heterogeneity, it can contribute to strength enhancement [121]; therefore given the evident lamellar structure shown in the EBSD micrographs in Figs. 4 and 6, it is reasonable to expect that back-stress could lead to enhanced mechanical properties. When GNDs are created to accommodate gradient strain and share the same Burgers vector, they pile up at the grain boundaries, creating stress concentrations at these sites. The resulting GND pile-up bends the slip plane and produces an internal long-range stress in the opposite direction of the applied stress, known as back stress [122,123]. This back stress prevents the emission of additional dislocations from the Frank-Read source, thus increasing the material's strength.

Another key factor that influences mechanical properties is grain refinement. Based on the well-documented Hall-Petch [3,43,124] relationship, a reduction in grain size results in increased strength because the greater density of grain boundaries obstructs dislocation movement, which is in a good agreement with the results obtained from EBSD analysis. Regarding this, it is worth mentioning that, as stated above, grain boundaries with higher misorientation angles (i.e. HAGBs) act as stronger barriers to dislocation motion in compression compared to those with lower misorientation angles (i.e. LAGBs). Thus, the enhancement of mechanical properties after the second pass can mainly be attributed to the increase in the fraction of HAGBs. Notably, as shown in Fig. 7, the Al sample subjected to a third pass of HTE did not exhibit substantial changes in mechanical properties; they remained almost unchanged following the second pass. It is noticing worthy that after the initial pass of HTE, there is a notable rise in YS (about 29.5 % increase) and UTS (about 29 % increase), but during higher strains observed after the second pass, this increase becomes less pronounced (about 7 % and 14 % increase in UTS and YS, respectively), and both strengths trend toward saturation levels (e.g. third pass). In this context, it has been confirmed that the annihilation of dislocations through dislocation core diffusion or grain boundary diffusion is the key factor behind yield and ultimate strengths approaching saturation levels [125]. Put another way, the steady state or saturation condition is influenced by the equilibrium between the hardening rate due to dislocation creation and the recovery rate that causes the annihilation and recombination of dislocations [89,126]. It was stated that at significant accumulated strains (e.g., during the third pass of HTE), the elimination of dislocations is primarily driven by the cross-slip of screw dislocations or the climb of edge dislocations [96,127,128]. As a case in point, the transmission electron microscopy (TEM) analysis conducted by Faraji et al. [88] showed that as the number of parallel tubular channel angular pressing (PTCAP) passes rises (i.e. accumulated plastic strain increases), the density of dislocations inside the grains diminishes. This phenomenon is clearly illustrated in Fig. 5d and Table 2, where the dislocation density significantly decreases from 9.34×10^{12} m^{-2} in the one-pass HTE-processed sample to 7.56×10^{12} m^{-2} in the three-pass HTE-processed sample. The steady-state behavior of mechanical properties, grain size, composition of phases etc. resulting from an increased number of passes has been reported by numerous researchers in the field of SPD [82,129–133].

On the other hand, ductility demonstrates a tendency to decline when the HTE process is applied, and this decrease becomes more evident with a greater number of passes, see Fig. 7. Ductility decreases from 28 % in the initial state to 24 % after the first pass and to 21.5 % after the second pass. It is worth noting that, similar to strength, the third pass did not significantly affect ductility. The ductility-strength paradox is a well-recognized phenomenon, frequently documented in numerous studies related to SPD [52,53,100,134]. Concerning this it was stated that, the primary cause of reduced ductility is the combination of elevated flow stress and the limited strain-hardening ability of materials processed by SPD [1,89]. One way to address this issue is by applying a high level of hydrostatic pressure to the sample [48,124], which effectively closes cracks and microvoids, thereby delaying the onset of cracking [27,135,136]. Indeed, the application of high compressive stress to the sample led to a remarkable combination of strength and ductility, allowing for simultaneous strength gains with only a slight loss in ductility. In this context, Orlov et al. [66] investigated the mechanical properties of pure aluminum after subjecting it to various passes of conventional TE. The findings revealed that UTS increased by 15 % following the first pass and by 2 % after the second pass, while total ductility experienced a dramatic reduction of about 50 % after the first pass and approximately 5 % after the second. However, as noted above, after one pass of the HTE process, the UTS shows an increase of 29 %, whereas total ductility exhibits a decrease of just 14 %. Fig. 8a illustrates the ductility loss values of the HTE-processed samples compared to those from other studies on pure Al, including 1-pass rubber pad tube straining (RPTS) [137], 1-pass accumulative back extrusion (ABE) [52], 5-pass tube channel pressing (TCP) [62], 2-pass ECAP (route A) [138], 2-pass ECAP (route C) [138], 3-pass ECAP (route C) [138], and 1-pass TE [66]. To better demonstrate the efficiency of the HTE process relative to other SPD techniques, Fig. 8b showcases a comparative analysis by plotting the UTS increment ($\frac{UTS_{Final}-UTS_{Initial}}{UTS_{Initial}}$) against the elongation reduction ($\frac{Elongation_{Final}-Elongation_{Initial}}{Elongation_{Initial}}$). It is evident that, apart from REU, which led to an almost 100 % increase in UTS accompanied by nearly a 70 % reduction in ductility, other SPD methods primarily resulted in a UTS enhancement ranging from 20 % to 40 % for CP Al. Additionally, although the HTE process enhances strength by approximately 40 %, the elongation reduction is kept below 30 %, which is notably less than that observed in TE, RPTS, and ECAR, all of which induce a comparable strength improvement, see Fig. 8b. As it is obvious, the application of high hydrostatic pressure during HTE caused only a slight decrease in ductility, unlike other conventional SPD-processed samples. This can be seen as a key advantage of the HTE process, where significant grain refinement is achieved with only a minimal loss of ductility.

A hardness test was carried out to further assess the mechanical properties of the HTE processed sample. Fig. 9a–d illustrates the microhardness contours of the color-coded contour maps of the hardness distributions over the cross-section of the annealed sample and the processed samples after different passes of the HTE process. The illustration indicates that the microhardness in the sample's center is lower than that on the periphery, attributed to the non-uniform distribution of strain from the deformation area [48,55]. Concerning this, it was found that most SPD techniques exhibit a degree of inhomogeneous strain distribution [66,139], which contributes to variations in microstructure and, consequently, in hardness [134]. During the initial phase of deformation, the outer regions (e.g., edges and corners) undergo greater imposed strain than the central regions, resulting in more pronounced grain refinement and, thus, higher hardness in these areas, as shown in Fig. 9b. However, because grain refinement occurs at a faster rate in the outer regions, they will achieve a saturated condition sooner than the central regions. Therefore, the increase in hardness in the outer regions diminishes with further straining, as after a specific deformation level, the strain only converts elongated grains to equiaxed grains, resulting in minimal changes to mechanical properties [78]. In contrast, applying a greater number of passes, as shown in Fig. 9c, leads to a decrease in grain size within the central regions, which in turn improves hardness. Furthermore, it is evident that a single pass of HTE results in a substantial increase in hardness value, rising from about 25.6 HV for the

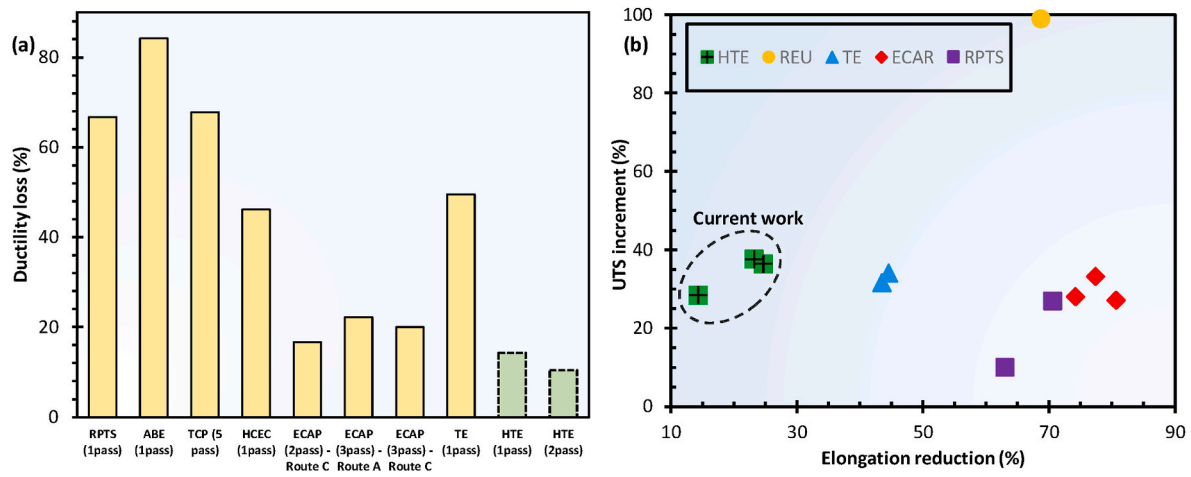

Fig. 8. a) Ductility loss of pure Al samples processed via various SPD methods (data are gathered from Ref.s [52,62,66,137,138]) and b) plot of UTS increment (%) versus elongation reduction (%) for various processing methods applied to Al 1xxx (data are gathered from Ref.s [57,66,134,137]).

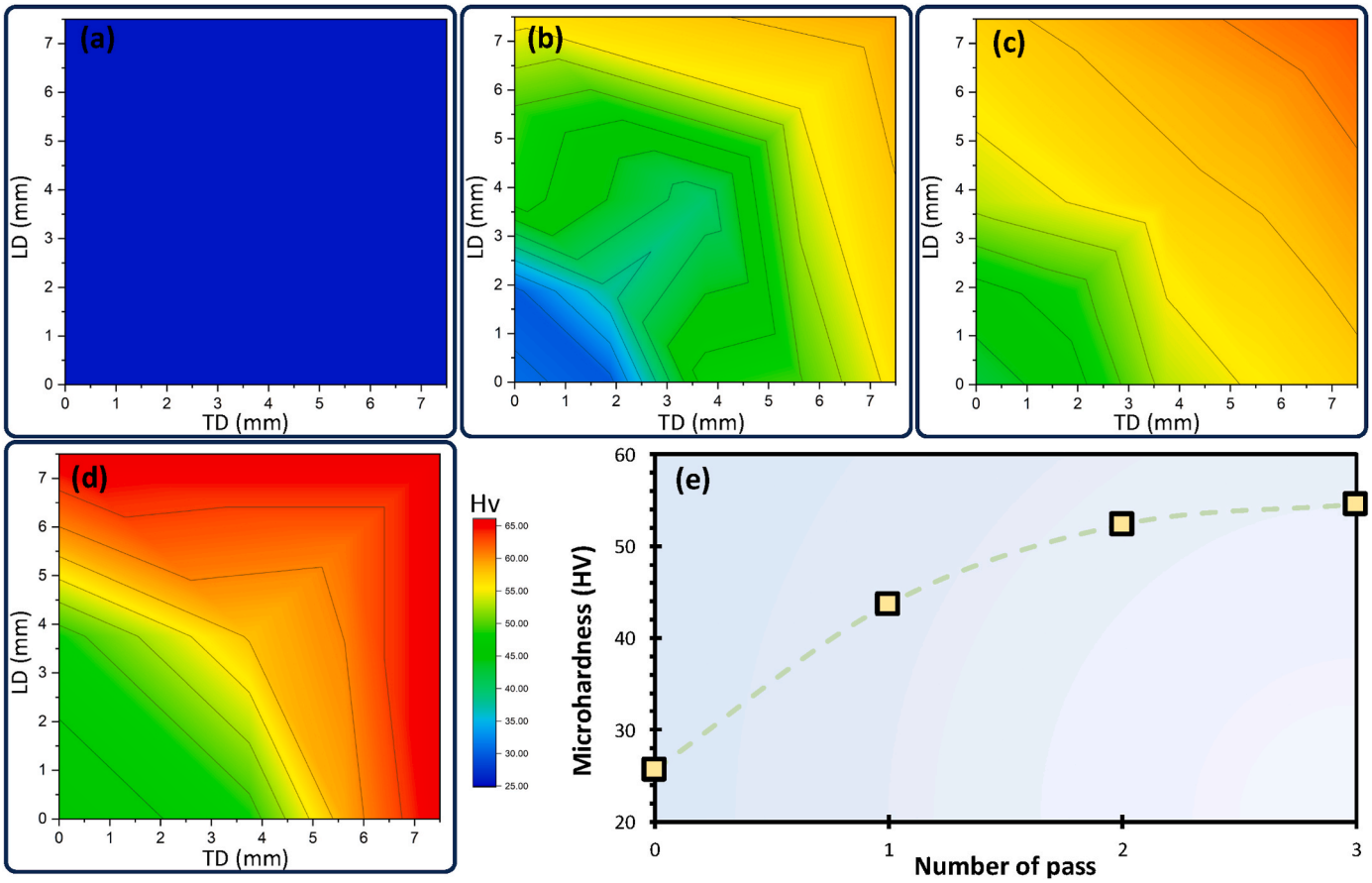

Fig. 9. The contour of microhardness related to one fourth of a) annealed sample, b) one pass HTE processed sample, c) two passes HTE processed sample, d) three passes HTE processed sample, and e) the average hardness value achieved through various passes of the HTE process.

annealed sample to nearly 43.7 HV, see Fig. 9d. Similar behavior has also been observed via other researchers [25,100,140]. The increased hardness in UFG metals is largely a result of the reduced grain size along with the enhanced multiplication and accumulation of dislocations [141], as indicated by EBSD images. The hardness value shows increase of 70 %, and 19 % following the first, and second passes of HTE, respectively. According to Fig. 9d, the variation in average hardness values pronounced as the number of passes increases, which aligns well with the findings from the tensile tests. Such behavior also supports the notion that a steady-state condition occurs.

3.3. Fractography

Fig. 10 displays the image of a fractured tensile sample along with its corresponding FESEM micrograph of the cross section before and after HTE processing. The presence of numerous deep dimples on the fracture surface of the samples signifies that a ductile fracture has occurred. In the ductile fracture mode, the creation of microvoids and dimples causes

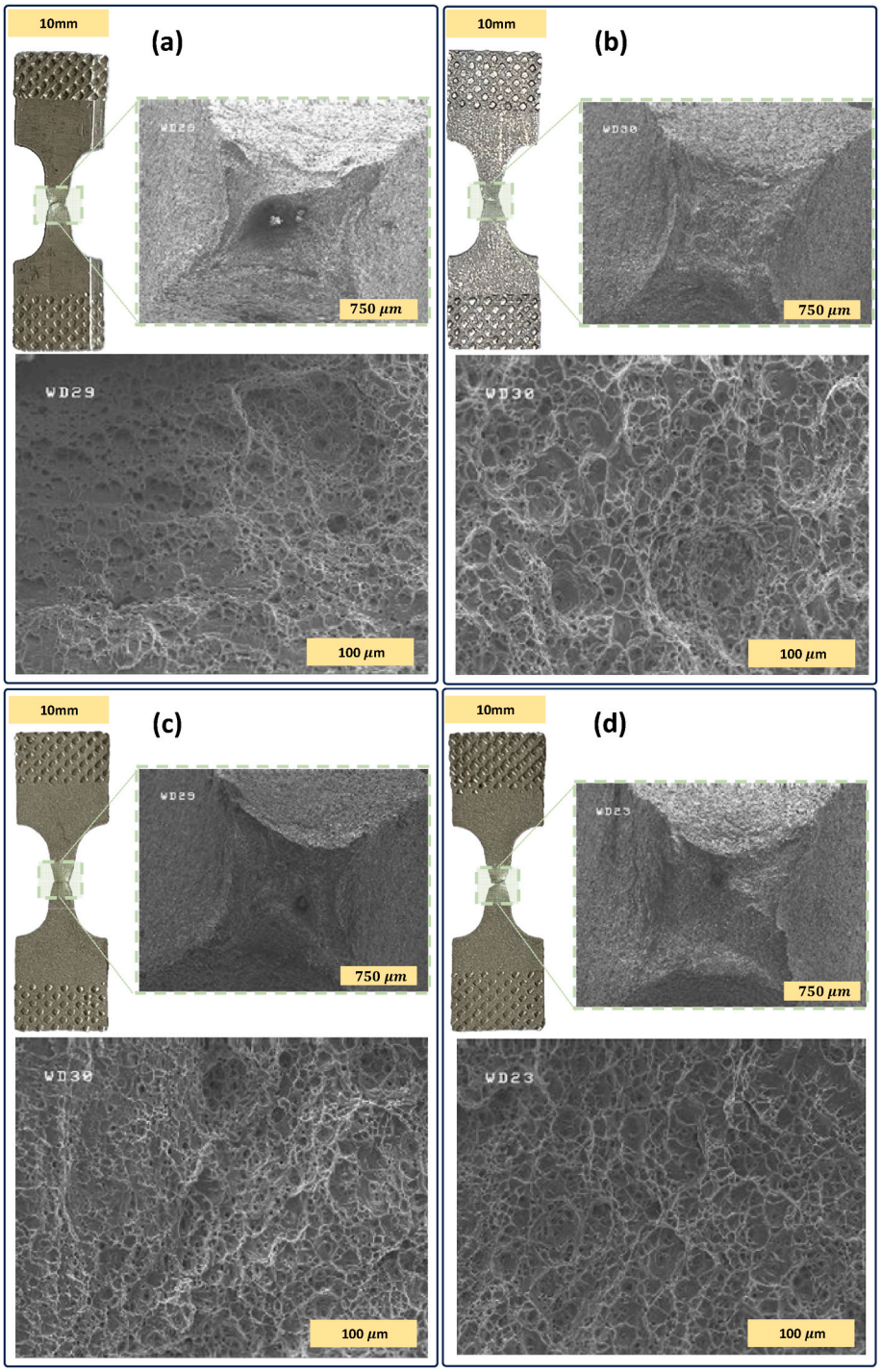

Fig. 10. Image of fractured tensile test and FESEM fractography related to a) annealed sample, b) one pass HTE processed sample, c) two passes HTE processed sample, d) three passes HTE processed sample.

crack development, ultimately leading to shear rupture at an angle to the tensile direction [16,], which is commonly observed in materials with an FCC crystalline structure [53,108,142]. According to Fig. 10, the fracture surface of the annealed specimen features dimples that are larger and deeper than those of the HTE processed specimens. On the other hand as the number of HTE passes increases, leading to a greater imposed plastic strain, the large dimples found in the annealed sample transform into smaller, shallower ones, see Fig. 10b and c. Several researchers have noted the same phenomenon in their studies [17,142]. Regarding this Faraji et al. [53] observed that the ultra-fine grained (UFG) material exhibits shallower dimples compared to the deep holes seen in the annealed sample, a change attributed to reduced ductility during SPD, which is linked to limited dislocation movement in the ultra-fine grains. The results from tensile testing reveal that the HTE process reduces uniform elongation and ductility, negatively impacting the work hardening capability, see Fig. 7. This means that in HTE processed samples, the dimples that form do not have sufficient time to enlarge and merge, causing them to be shallower, which can be seen in Fig. 10.

4. Conclusions

Hydrostatic Twist Extrusion (HTE) has been demonstrated in this study as a novel and efficient Severe Plastic Deformation (SPD) method for refining ultrahigh aspect ratio pure aluminum. The results indicate that HTE enables superior grain refinement and mechanical strengthening, offering advantages over conventional SPD techniques. EBSD analysis demonstrated that two passes of HTE resulted in significant grain refinement and lamellar structure formation, effectively reducing the grain size from approximately 99 μm–4.9 μm. The application of high hydrostatic pressure during HTE processing led to the formation of a high fraction of HAGBs, with the first pass achieving a 33.4 % HAGB fraction, which increased by 70 % after the second pass. Furthermore, microhardness measurements revealed a substantial enhancement in the mechanical properties of the processed aluminum billets, increasing from 25.6 HV initially to 43.7 HV after the first pass and reaching 52.36 HV after two passes. The enhancement in microhardness reflects the effectiveness of HTE in strengthening the material while simultaneously maintaining a reasonable level of ductility, with losses of 14 % after the first pass and 10 % after the second. The minimal reduction in ductility alongside the substantial strength gain in HTE-processed aluminum is attributed to the effective combination of grain boundary strengthening, dislocation interactions, and the high hydrostatic pressure used during processing, offering a balanced enhancement of both strength and ductility.

Declaration of competing interest

The authors declare that they have no known competing financial interests or personal relationships that could have appeared to influence the work reported in this paper.

References

[1] Estrin Y, Vinogradov A. Acta Mater 2013;61:782–817.
[2] Azushima A, Kopp R, Korhonen A, Yang D-Y, Micari F, Lahoti G, Groche P, Yanagimoto J, Tsuji N, Rosochowski A. CIRP Annal 2008;57:716–35.
[3] Edalati K, Ahmed AQ, Akrami S, Ameyama K, Aptukov V, Asfandiyarov RN, Ashida M, Astanin V, Bachmaier A, Beloshenko V. J Alloys Compd 2024:174667.
[4] El-Garhy G, El Mahallawy N, Shoukry M. J Mater Res Technol 2021;12:1886–97.
[5] Valiev RZ, Estrin Y, Horita Z, Langdon TG, Zechetbauer MJ, Zhu YT. Jom 2006; 58:33–9.
[6] Valiev RZ, Langdon TG. Prog Mater Sci 2006;51:881–981.
[7] Segal V. Patent of the USSR 575892. 1977. p. 330.
[8] Rassa M, Azadkoli G, Eftekhari M, Fata A, Faraji G. J Advan Mater Process 2021; 9:43–52.
[9] Radnia A, Ketabchi M, He A, Li D. J Mater Res Technol 2025.
[10] Berndt N, Reiser NA, Wagner MF-X. J Mater Res Technol 2025;34:359–71.
[11] Al-Zubaydi A, Figueiredo RB, Huang Y, Langdon TG. J Mater Sci 2013;48: 4661–70.
[12] Naumova E, Rogachev S, Sundeev R. J Alloys Compd 2021;854:157117.
[13] Rogachev S, Sundeev R, Nikulin S. J Alloys Compd 2021;865:158874.
[14] Eskandarzade M, Masoumi A, Faraji G, Mohammadpour M, Yan XS. J Alloys Compd 2017;695:1539–46.
[15] Ivanisenko Y, Kulagin R, Fedorov V, Mazilkin A, Scherer T, Baretzky B, Hahn H. Mater Sci Eng, A 2016;664:247–56.
[16] Rahmatabadi D, Tayyebi M, Hashemi R, Faraji G. Powder Metall Met Ceram 2018;57:144–53.
[17] Sadrkhah M, Faraji G, Esmaeili V. JOM 2023;75:5628-5642.
[18] Saito Y, Utsunomiya H, Tsuji N, Sakai T. Acta Mater 1999;47:579-583.
[19] Richert J. Aliminum 1986;62:604–7.
[20] Lin J, Wang Q, Peng L, Roven HJ. J Alloys Compd 2009;476:441–5.
[21] Tian Y, Huang H, Yuan G, Ding W. J Alloys Compd 2015;626:42–8.
[22] Beygelzimer Y, Orlov D, Varyukhin V. A new severe plastic deformation method: twist extrusion. Ultrafine Grain Mater II 2002;2002:297–304.
[23] Attarilar S, Gode C, Mashhuriazar M, Ebrahimi M. J Alloys Compd 2021;859: 157855.
[24] Pardis N, Talebanpour B, Ebrahimi R, Zomorodian S. Mater Sci Eng, A 2011;528: 7537–40.
[25] Savarabadi MM, Faraji G, Zalnezhad E. J Alloys Compd 2019;785:163–8.
[26] Faraji G, Mashhadi MM, Kim HS. Mater Lett 2011;65:3009–12.
[27] Faraji G, Kim H. Mater Sci Technol 2017;33:905–23.
[28] Mishra RS, Ma Z, Charit I. Mater Sci Eng, A 2003;341:307–10.
[29] Arora H, Singh H, Dhindaw B. Int J Adv Des Manuf Technol 2012;61:1043–55.
[30] Pouraliakbar H, Jandaghi MR, Aval HJ, Shim SH, Moverare J, Na Y-S, Khalaj G, Fallah V. J Mater Res Technol 2025;35:685–701.
[31] Kawalko J, Wronski M, Bieda M, Sztwiertnia K, Wierzbanowski K, Wojtas D, Lagoda M, Ostachowski P, Pachla W, Kulczyk M. Mater Char 2018;141:19–31.
[32] Kawałko J, Bobrowski P, Koprowski P, Jarzębska A, Bieda M, Łagoda M, Sztwiertnia K. J Alloys Compd 2017;707:298–303.
[33] Pachla W, Kulczyk M, Sus-Ryszkowska M, Mazur A, Kurzydlowski KJ. J Mater Process Technol 2008;205:173–82.
[34] Wojtas D, Wierzbanowski K, Chulist R, Pachla W, Bieda-Niemiec M, Jarzębska A, Maj Ł, Kawałko J, Marciszko-Wiąckowska M, Wroński M. J Alloys Compd 2020; 837:155576.
[35] Hall E. Nature 1954;173:948–9.
[36] Hall E. Proc Phys Soc B 1951;64:747.
[37] Valiev RZ, Langdon TG. Metall Mater Trans 2011;42:2942–51.
[38] Segal V. Mater Sci Eng, A 1995;197:157–64.
[39] Bridgman PW. Phys Rev 1935;48:825.
[40] Bridgman PW. Studies in large plastic flow and fracture: with special emphasis on the effects of hydrostatic pressure. Harvard University Press; 1964.
[41] Valiev R, Kuznetsov O, Musalimov RS, Tsenev N. Low-temperature superplasticity of metallic materials. Sov Phys Dokl 1988;33:626.
[42] Valiev RZ, Krasilnikov N, Tsenev N. Mater Sci Eng, A 1991;137:35–40.
[43] Edalati K, Bachmaier A, Beloshenko VA, Beygelzimer Y, Blank VD, Botta WJ, Bryła K, Čížek J, Divinski S, Enikeev NA. Mater Res Letter 2022;10:163–256.
[44] Zehetbauer M, Grössinger R, Krenn H, Krystian M, Pippan R, Rogl P, Waitz T, Würschum R. Adv Eng Mater 2010;12:692–700.
[45] Taherkhani E, Sabour M, Faraji G. J Magnesium Alloys 2024.
[46] Sabour M, Taherkhani E, Rezaei A, Zohrevand M, Safahi H, Faraji G. J Mater Res Technol 2024.
[47] Derakhshan JF, Parsa M, Jafarian H. Mater Sci Eng, A 2019;747:120–9.
[48] Zohrevand M, Rezaei AR, Sabour MR, Taherkhani E, Faraji G. Mater Trans 2023; 64:1663–72.
[49] Tsai T, Sun P, Kao P, Chang C. Mater Sci Eng, A 2003;342:144–51.
[50] Wang Y, Ma E. Acta Mater 2004;52:1699–709.
[51] Siahsarani A, Faraji G. Arch Civ Mech Eng 2020;20:1–13.
[52] Haghdadi N, Zarei-Hanzaki A, Abou-Ras D. Mater Sci Eng, A 2013;584:73–81.
[53] Faraji G, Roostae S, Seyyed Nosrati A, Kang J, Kim H. Metall Mater Trans 2015; 46:1805–13.
[54] Faraji G, Taherkhani E, Sabour MR. Cyclic severe plastic deformation processes. In: Hashmi S, editor. Comprehensive Materials Processing. 3. Elsevier; 2023. p. 105–29.
[55] Haghpanah M, Esmaeilnia A, Sabour M, Taherkhani E, Mashhadi MM, Faraji G. Mater Lett 2023;333:133660.
[56] Alihosseini H, Faraji G, Dizaji A, Dehghani K. Mater Char 2012;68:14–21.
[57] Zaharia L, Comaneci R, Chelariu R, Luca D. Mater Sci Eng, A 2014;595:135–42.
[58] Richert M, Liu Q, Hansen N. Mater Sci Eng, A 1999;260:275–83.
[59] Pardis N, Chen C, Shahbaz M, Ebrahimi R, Toth LS. Mater Sci Eng, A 2014;613: 357–64.
[60] Babaei A, Mashhadi M, Mehri Sofiani F. Proc Inst Mech Eng Part L 2018;232: 481–94.
[61] Mesbah M, Faraji G, Bushroa AR. Mater Sci Eng, A 2014;590:289–94.
[62] Zangiabadi A, Kazeminezhad M. Mater Sci Eng, A 2011;528:5066–72.
[63] Li J, Li F, Ma X, Chen H, Ma Z, Li J. J Mater Eng Perform 2015;24:4543–50.
[64] Su L, Deng G, Luzin V, Wang H, Wang Z, Yu H, Li H, Tieu AK. Mater Sci Eng, A 2020;780:139190.
[65] Beygelzimer Y, Prilepo D, Kulagin R, Grishaev V, Abramova O, Varyukhin V, Kulakov M. J Mater Process Technol 2011;211:522–9.
[66] Orlov D, Beygelzimer Y, Synkov S, Varyukhin V, Tsuji N, Horita Z. Mater Sci Eng, A 2009;519:105–11.
[67] Faraji G, Mashhadi MM, Joo S-H, Kim HS. Rev Adv Mater Sci 2012;31:12–8.
[68] Siahsarani A, Faraji G. Trans Nonferrous Metals Soc China 2021;31:1303–21.
[69] Samadpour F, Faraji G, Siahsarani A. Int J Miner Metall Mater 2020;27:669–77.
[70] Canadinc D, Biyikli E, Niendorf T, Maier HJ. Adv Eng Mater 2011;13:281–7.
[71] Beygelzimer Y, Varyukhin V, Synkov S, Orlov D. Mater Sci Eng, A 2009;503:14–7.
[72] Berta M, Orlov D, Prangnell PB. Int J Mater Res 2007;98:200–4.
[73] Bay B, Hansen N, Hughes D, Kuhlmann-Wilsdorf D. Acta Metall Mater 1992;40: 205–19.
[74] Kocks U, Canova G. Riso National Laboratory. 1981. p. 35–44. Roskilde.
[75] Tham Y, Fu M, Hng H, Pei Q, Lim K. Mater Manuf Process 2007;22:819–24.
[76] Cottrell A. Dislocations and plastic flow in crystals. Clarendon press; 1956.
[77] Meyers MA, Chawla KK. Mechanical behavior of materials. Cambridge university press; 2008.
[78] Cao Y, Ni S, Liao X, Song M, Zhu Y. Mater Sci Eng R Rep 2018;133:1–59.
[79] An X, Wu S, Wang Z, Zhang Z. Prog Mater Sci 2019;101:1–45.
[80] Muzyk M, Pakiela Z, Kurzydlowski K. Scr Mater 2011;64:916–8.
[81] Hardwick D, Sellars C, Tegart W. The occurrence of recrystallization during high-temperature creep. In: Inst materials 1 carlton house terrace, vol. 90; 1961. p. 21–2. LONDON SW1Y 5DB, ENGLAND.
[82] Eftekhari M, Faraji G, Bahrami M. Arch Civ Mech Eng 2021;21:1–12.
[83] Eftekhari M, Faraji G, Nikbakht S, Rashed R, Sharifzadeh R, Hildyard R, Mohammadpour M. Mater Sci Eng, A 2017;703:551–8.
[84] Tavakkoli V, Boltynjuk E, Scherer T, Mazilkin A, Ivanisenko Y, Ungar T, Kübel C. Mater Sci Eng, A 2024:146556.
[85] Kuhlmann-Wilsdorf D. Mater Sci Eng, A 1989;113:1–41.
[86] Hansen N, Kuhlmann-Wilsdorf D. Mater Sci Eng 1986;81:141–61.
[87] Hughes D, Hansen N, Bammann D. Scr Mater 2003;48:147–53.
[88] Faraji G, Mashhadi MM, Bushroa AR, Babaei A. Mater Sci Eng, A 2013;563:193–8.
[89] Faraji G, Kim HS, Kashi HT. Severe plastic deformation: methods, processing and properties. Elsevier; 2018.

[90] Bay B, Hansen N. Math Sci Eng 1989;Al13:385–97.
[91] Taylor GI. J Inst Met 1938;62:307–24.
[92] Hull D, Bacon DJ. Introduction to dislocations. Elsevier; 2011.
[93] N⊘ st B. Philos Mag 1965;11:183–4.
[94] Jata K, Semiatin SL. Scr Mater 2000;43:743–9.
[95] Orlov D, Beygelzimer Y, Synkov S, Varyukhin V, Horita Z. Mater Trans 2008;49:2–6.
[96] Mckenzie PWJ, Lapovok R, Estrin Y. Acta Mater 2007;55:2985–93.
[97] Hughes D, Hansen N. Metall Trans A 1993;24:2022–37.
[98] Winther G, Huang X. Philos Mag 2007;87:5215–35.
[99] Huang X-x, Winther G. Philos Mag 2007;87:5189–214.
[100] Samadpour F, Faraji G, Babaie P, Bewsher S, Mohammadpour M. Mater Sci Eng, A 2018;718:412–7.
[101] Chen Y, Li Y, He L, Lu C, Ding H, Li Q. Mater Lett 2008;62:2821–4.
[102] Zhang H, Huang X, Hansen N. Acta Mater 2008;56:5451–65.
[103] Doherty R, Hughes D, Humphreys F, Jonas JJ, Jensen DJ, Kassner M, King W, McNelley T, McQueen H, Rollett A. Mater Sci Eng, A 1997;238:219–74.
[104] Wang Y, Zhang X, Chen T. J Alloys Compd 2023;930:167456.
[105] Hughes D, Hansen N. Acta Mater 1997;45:3871–86.
[106] Kuhlmann-Wilsdorf D, Hansen N. Scripta Metall Mater 1991;25:1557–62.
[107] Ito Y, Horita Z. Mater Sci Eng, A 2009;503:32–6.
[108] Mishra A, Kad B, Gregori F, Meyers M. Acta Mater 2007;55:13–28.
[109] Meiser H, Gleiter H, Mirwald R. Scripta Metall 1980;14:95–9.
[110] Jahedi M, Beyerlein IJ, Paydar MH, Zheng S, Xiong T, Knezevic M. Metall Mater Trans 2017;48:1249–63.
[111] Guan W, Linyuan K, Zhiwen L, Shikang L, Luoxing L. Mater Res Express 2019;6:056555.
[112] Quan G-Z, Liu K-W, Jie Z, Bin C. Trans Nonferrous Metals Soc China 2009;19:s537–41.
[113] Driver J. Mater Lett 2018;222:135–7.
[114] Motallebi Savarabadi M, Faraji G, Eftekhari M. Met Mater Int 2021;27:1686–700.
[115] Niendorf T, Dadda J, Canadinc D, Maier H, Karaman I. Mater Sci Eng, A 2009;517:225–34.
[116] Sun P, Cerreta E, Bingert J, Gray III G, Hundley M. Mater Sci Eng, A 2007;464:343–50.
[117] Jamaati R, Toroghinejad MR. Mater Des 2010;31:4816–22.
[118] Chinh NQ, Csanádi T, Gubicza J, Langdon TG. Acta Mater 2010;58:5015–21.
[119] Kuhlmann-Wilsdorf D. Scr Mater 1997;36:173–81.
[120] Phan TQ, Levine LE, Lee I-F, Xu R, Tischler JZ, Huang Y, Langdon TG, Kassner ME. Acta Mater 2016;112:231–41.
[121] Wu X, Zhu Y, Lu K. Scr Mater 2020;186:321–5.
[122] Mughrabi H. Mater Sci Eng, A 2001;319:139–43.
[123] Zhu Y, Wu X. Mater Res Letter 2019;7:393–8.
[124] Faraji G, Taherkhani E, Sabour MR. Cyclic severe plastic deformation processes, Comprehensive Materials Processing. Elsevier; 2024. p. 105–29.
[125] Edalati K, Fujioka T, Horita Z. Mater Sci Eng, A 2008;497:168–73.
[126] Mohamed FA. Acta Mater 2003;51:4107–19.
[127] Zehetbauer M. Acta Metall Mater 1993;41:589–99.
[128] Zehetbauer M, Stüwe H-P, Vorhauer A, Schafler E, Kohout J. Adv Eng Mater 2003;5:330–7.
[129] Babaei A, Mashhadi M. Prog Nat Sci: Mater Int 2014;24:623–30.
[130] Majidabad MA, Rezaei A, Sabour M, Faraji G. J Ultrafine Grained Nanostruct Mater 2023;56.
[131] Straumal BB, Kilmametov AR, Ivanisenko Y, Mazilkin AA, Kogtenkova OA, Kurmanaeva L, Korneva A, Zięba P, Baretzky B. Int J Mater Res 2015;106:657–64.
[132] Straumal BB, Kulagin R, Klinger L, Rabkin E, Straumal PB, Kogtenkova OA, Baretzky B. Materials 2022;15:601.
[133] Straumal B, Kilmametov A, Straumal P, Mazilkin A. J Mater Sci 2024:1–13.
[134] Azimi A, Tutunchilar S, Faraji G, Givi MB. Mater Des 2012;42:388–94.
[135] Lapovok RY. J Mater Sci 2005;40:341–6.
[136] Lapovok R. The positive role of back-pressure in equal channel angular extrusion. Mater Sci Forum 2006;503:37–44. Trans Tech Publ.
[137] Shapourgan O, Faraji G. Proc IME B J Eng Manufact 2016;230:1845–54.
[138] Surendarnath S, Sankaranarayanasamy K, Ravisankar B. Mater Manuf Process 2014;29:691–6.
[139] Amani S, Faraji G, Abrinia K. J Manuf Process 2017;28:197–208.
[140] Jamali S, Faraji G, Abrinia K. Int J Adv Des Manuf Technol 2017;88:291–301.
[141] Mesbah M, Faraji G, Bushroa A. Met Mater Int 2016;22:288–94.
[142] Afrasiab M, Faraji G, Tavakkoli V, Mashhadi M, Dehghani K. Trans Indian Inst Met 2015;68:873–9.